Mecánica Computacional Vol. XXI, pp. 2923–2944
S. R. Idelsohn, V. E. Sonzogni and A. Cardona (Eds.)
Santa Fe–Paraná, Argentina, October 2002

ELECTROCHEMICAL INTERCONNECTIONS: HYDRODYNAMIC, GROWTH PATTERNS AND CONTACT MORPHOLOGY. EXPERIMENTAL, THEORETICAL, AND PARALLEL COMPUTATIONAL SIMULATION STUDIES

G. Marshall*, F. V. Molina†, G. Gonzalez*†, S. Dengra*, E. Arias*, E. Mocskos*, F. Daffara* and R. Fernandez*

*Departamento de Computacion
FCEN, Universidad de Buenos Aires,
1428 Buenos Aires, Argentina
†INQUIMAE,
FCEN, Universidad de Buenos Aires,
1428 Buenos Aires, Argentina

Key Words: Electrodeposition, thin-layer, ionic transport, gravitoconvection, electroconvection, bipolar electrochemistry, pulsed field.

Abstract. *Ion transport and growth morphology in monopolar and bipolar ramified deposits in thin-layer cells, under constant and periodic electric field pulses, are studied through experimental measurements and theoretical and computational modeling. The use of optical techniques and micron sized particle image velocimetry, allow the tracking of the convection, migration and concentration fronts, the determination of incubation and contact times and the measurement of fluid velocity. The theoretical macroscopic model describes the diffusive, migratory and convective motion of ions in a fluid subject to an electric field. The equations are written in terms of 13 dimensionless quantities, in particular, the Migration, Poisson, Reynolds and Electric and Gravity Grashof numbers, which values determine the prevailing ion transport mode and thus the characteristic of the ramified deposit. Numerical simulations in realistic cell configurations using serial and parallel computing are presented. Theory and simulations predict full front interaction, vortex generation and merging and a space-time fronts evolution, in close agreement with the results observed in the experiments.*

1 INTRODUCTION

Electrochemical deposition of metals is a very ancient topic with a wide range of industrial applications. Since long, chemists knew how to control the deposit growth and form. However, in recent years monopolar electrodeposition in thin-layer cells (ECD) under constant electric fields was the subject of renewed interest as a paradigmatic model for the study of pattern formation during growth.[1,2] A closely related problem in bipolar electrochemistry under constant electric fields, known as Spatially Coupled Bipolar Electrochemistry (SCBE) has been recently introduced.[3,4] In SCBE electrodissolution and electrodeposition in an applied electric field can be exploited to create directional growth of copper deposits between copper particles that are not connected to an external circuit. The study of monopolar and bipolar electrochemistry in thin-layer cells under alternating voltage conditions and its effects upon ion transport has very recently been addressed;[5,6] electric field and ion transport constitute crucial factors in the characteristics of the connection.

In monopolar ECD, the electrolytic cell consists of two glass plates sandwiching two parallel electrodes and a metal salt electrolyte. A voltage difference applied between electrodes produces a treelike deposit by a reduction of the metal ions. The morphology of the deposit can be fractal, densely branched, or dendritic depending on the cell geometry, electrolyte concentration, cell voltage, and other parameters. Ion transport is mainly governed by diffusion, migration and convection. Convection is driven mainly by coulombic forces due to local charges and by buoyancy forces due to concentration gradients that lead to density gradients. The relevance of convection, relative to migration and diffusion, for cells with thickness larger than 50 m has been demonstrated by a number of researchers. In cells with thickness less than 50 m, diffusion and migration are the dominant modes in ion transport.

Changes in the growth rate and in the morphology of the deposit have been reported when fronts emanating from the anode encounters the deposit. The first pattern transition or Hecker effect is associated with a migratory pH front, a second pattern transition is due to the anodic convection front which travels at the same speed as the cathodic convection front -when it is not perturbed by the growing deposit.

Viscosity is a key parameter to analyze the influence of convection. A preliminary study analyzing the effects of viscosity changes in ECD was presented by Fleury et. al.[7] Gonzalez et al.[8,9] analyzed experimentally and theoretically the effects of viscosity on ion transport in ECD. Viscosity variations were obtained through the addition of glycerol; it was found experimentally that increasing viscosity concentration fronts slow down while electric resistance and voltage increased. The theoretical model presented describes diffusive, migratory and convective ion transport in a fluid subject to an electric field. Its prediction of the space-time evolution of fronts is remarkably close to measurements.

In bipolar SCBE, the electrolytic cell consists of two glass plates sandwiching two parallel Platinum electrodes at the two ends of the cell, two copper discs with a small

separation between them at the center of the cell and a dilute sulfuric acid electrolyte. An appropriate voltage difference applied between electrodes polarizes the copper discs inducing electrochemical reactions. Because a single disc acts simultaneously as cathode and anode, this process is called bipolar electrochemistry, as opposed to classical monopolar electrochemistry (ECD). In the region between discs, initially copper dissolution take place on the anodic side whereas hydrogen reduction is produced in the opposite side. After an initial period of time, the copper ion front reaches the opposite copper disc and electrodeposition starts producing a treelike deposit with complex morphology. Bradley et al.[4] presented an experimental and theoretical study of SCBE under constant voltage in which the ion transport and its effects on the morphology of the deposit was analyzed. It is shown that the electric field is almost one order of magnitude larger in the region between discs as compared with the mean field value. Monopolar electrochemistry in thin-layer cells under alternating voltage conditions has received little attention. In Zeiri et al.,[5] silver electrodeposits under alternating square-wave electric potential conditions were studied at the water /dichloromethane interface. It was shown that the deposit morphology strongly depends on frequency. In D'Angelo et al.[6] a study of SCBE in thin-layer cells under square-wave electric potential conditions was conducted. Some of these results corroborated the experimental measurements from Zeiri et al.[5] In this paper we review monopolar and bipolar electrochemical deposition experiments and theory and we study their analogies.

2 MONOPOLAR ELECTROCHEMISTRY

In a typical experiment, as current flows through a thin electrochemical cell, ion concentration boundary layers develop near both electrodes. At the anode, the concentration is increased above its initial level due to the transport of anions towards, and the dissolution of metal ions from, the anode. At the cathode, the ion concentration is decreased as metal ions are reduced and deposited out and anions drift away. These concentration variations lead to density variations, and so to the development of gravity-driven convection rolls at the electrodes. This flow was studied by Huth et al.[10] where a particle tracking technique was used to measure the convective velocity field. Figure 8 from Huth et al.[10] ilustrates this behavior.

Figure 3 from Huth et al.[10] depicts interferometric experimental measurements showing bands of constant density near the anode at early times. The isoconcentration bands are not parallel to the electrode surface due mainly to convection effects.

In Gonzalez et al.[8] the effects of viscosity on ion transport in ECD was analyzed through the addition of glycerol; viscosity variation ranging from ν_0 (viscosity of pure water) to 3.8 ν_0, were achieved through glycerol additions of 10, 20, 30 and 40 percent in weight, respectively. In solutions without glycerol, several studies have found that the convection rolls initially grow in size as $t^{4/5}$, while at later times the growth crossed over to a $t^{1/2}$ growth law. When viscosity increases, the same behavior is found as shown in Figure 1, although the curves are shifted towards higher times.

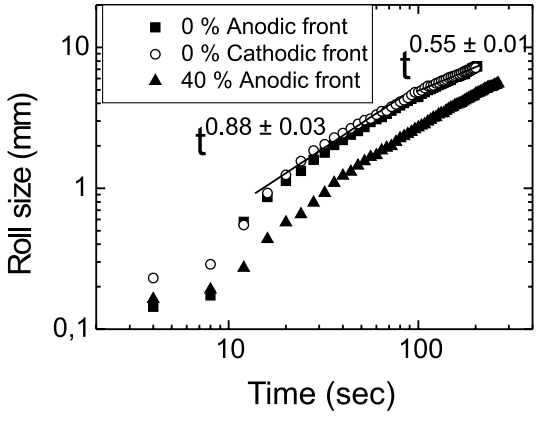

Figure 1: Roll size for anodic convective fronts as a function of time for different viscosities

It is possible to analyze the intensity of convective motion by particle tracking measurements. Figure 2 taken from Gonzalez et al.[9] shows a top view of the flow visualizing one micron sized particle trajectories near the deposit front in a horizontal plane. Several digital images spanning an interval of 10 seconds (left column: 0-10 sec, center column: 10-20 sec, right column: 20-30 sec) are superimposed and thresholded to show the motion of the tracer particles. From top down in each column, each frame represents a different value of glycerol concentration: 0, 20 and 40 percent w/w, respectively, yielding viscosities of 0, 1.8 0 and 3.8 0 respectively. In the top three frames, two regions are observed near the deposit front: a) a zone with a buoyancy driven convection dominated flow (the trajectories of particles, entrained in a vortex tube with an horizontal axis, are projected as lines in the plane of the cell, moving upwards near the deposit front and downwards in the zone limit); and b) a steady state region in which a brownian motion is observed. In the middle frames, due to an increase in viscosity, the gravitoconvection is attenuated and electroconvection prevails as observed (particle trajectories entrained toroidal vortex ring centered at a tip branch are projected as a circle in the plane of the cell). In the bottom frames the increase of viscosity produces a substantial damping of convection.

The relative importance of gravitoconvection and electroconvection can be assessed by measuring the velocity direction: in pure gravitoconvection a top view of the cell will show the projection of the vortex tube trajectories as lines normal to the cathode, while in pure electroconvection a top view will show circular trajectories. In Gonzalez et al.[2] it is shown that the distribution of particle directions for different angles (0 degree angle means motion parallel to the cathode) is given in such a way that for 0 percent glycerol the dominant direction is perpendicular to the electrode, indicating a gravitoconvective dominant regime. As viscosity is increased, for 40 percent glycerol the parallel and normal direction have similar weight, revealing a circular motion, and thus electroconvective prevailing conditions.

3 THEORETICAL AND NUMERICAL MODELING IN MONOPOLAR ELECTROCHEMISTRY

The phenomenological model discussed above can be described using the Nernst -Planck equations for transport of ions,[11] the Poisson equation for the electric potential, and the Navier-Stokes equations for the fluid flow. This model is an extension of the models introduced by Marshall et al,[12,13] The dimensionless system of equations is

$$\frac{\partial C_i}{\partial t} = -\nabla \cdot \mathbf{j}_i \tag{1}$$

$$\mathbf{j}_i = -M_i C_i \nabla \phi - \frac{1}{Pe_i} \nabla C_i + C_i \mathbf{v} \tag{2}$$

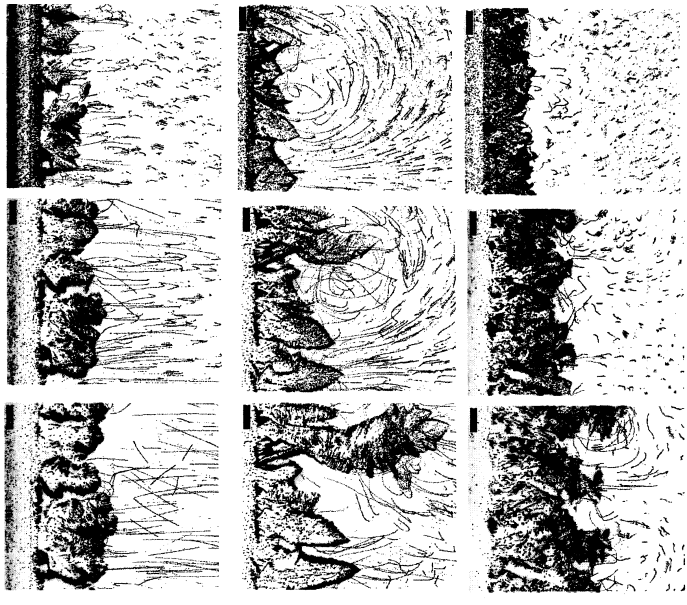

Figure 2: Top view cell visualization of 1 μ sized particle trajectories near the deposit front. In each frame, several digital images (spanning an interval of 10 seconds) were superimposed and thresholded. From left to right, each column represents a different time interval: left,0-10 s; center, 10-20 s; right, 20-30 s. From top down, each row corresponds to a different value of glycerol concentration: 0, 10, 20, 30 and 40 percent, respectively. Frame dimensions: 1.53 mm wide and 1.17 mm in height.

$$\nabla^2\phi = Po\sum_i z_i C_i \tag{3}$$

$$\frac{\partial \mathbf{v}}{\partial t} + \mathbf{v}\cdot\bigtriangledown\mathbf{v} = -\bigtriangledown P + \frac{1}{Re}\bigtriangledown^2\mathbf{v} + \left(\frac{1}{Fr} + \sum_i Gg_i\Delta C_i\right)\frac{\mathbf{g}}{g} + \mathbf{E}Ge\sum_i z_i C_i \tag{4}$$

$$\bigtriangledown\cdot\mathbf{v} = 0 \tag{5}$$

Here C_i and $\mathbf{j}_i$ are the dimensionless concentration and flux of an ionic species i (for a ternary electrolyte such as $ZnSO_4$ /H_2SO_4, i= C, A and H, standing for zinc, sulphate and hydrogen ions); $\mathbf{v}$, ϕ, P and $\mathbf{E}$ are the dimensionless fluid velocity, electrostatic potential, pressure and electric field, respectively; $\mathbf{g}/g$ is a unit vector pointing in the direction of gravity. The dimensionless numbers are defined in Gonzalez et al.[8] There, the quantities z_i, μ_i, and D_i are, respectively, the number of charges per ion, mobility and diffusion constants of an ionic species i; μ_i and z_i are signed quantities, being positive for cations and negative for anions; g is the dimensional gravitational acceleration; e is the electronic charge, ϵ is the permittivity of the medium and ν is the kinematic viscosity. x_0, u_0, ϕ_0, C_0, and ρ_0 are reference values of the length, velocity, electrostatic potential, concentration, and fluid density, respectively. For system closure, a Boussinesq-like approximation has been used for the fluid density: $\rho = \rho_o(1 + \Sigma_i\alpha_i\Delta C_i)$, where $\alpha_i = \frac{1}{\rho_o}\frac{\partial\rho}{\partial C_i}$.

The three-dimensional model presented above can be treated as a set of two bidimensional models in a horizontal and a vertical plane, respectively[12] . The horizontal plane model constitutes what we called the top view model while the vertical plane model constitutes the side view model. These models simulate the limiting cases of electrical driven or gravity driven convection prevailing regimes, respectively. The computational model solves the previous system, for each time step, in a fixed domain, in a 2D uniform lattice (equal spacing in both directions) using finite differences and deterministic relaxation techniques. The computational model is implemented using domain decomposition in a parallel architecture computer consisting in a cluster of 4 PC's connected with fast ethernet under Linux and MPI (Message Passing Interface).[14] The numerical implementation achieved almost linear speedup.

Figure 3 presents snapshots of a side view model simulation of the space time evolution of the contour lines of the stream function for no added glycerol. This picture shows vividly the existence and space-time evolution of cathodic and anodic vortex rolls. The region entrained by the buoyancy driven convection grows with time, invading the cell from both ends as shown by this figure. They continue growing until they collide. This modifies significantly the flow pattern and the ion concentration. Between the vortex rolls there is no motion prior to vortex collision, afterwards the fluid is entrained in one single vortex.

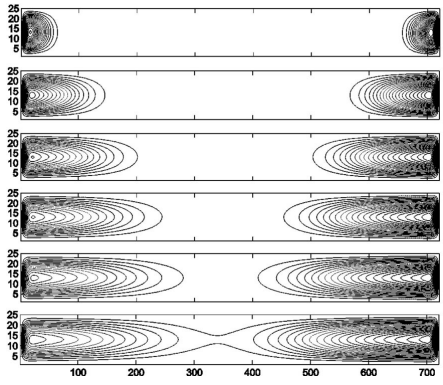

Figure 3: Space time evolution of the contour lines of the stream function for no added glycerol.

This figure can be qualitatively compared with the experimental rolls of Figure 8 from Huth et al.[10] .

Figure 4 shows the space time evolution of the contour lines of the dimensionless cation concentration for no added glycerol. Concentration is affected by gravitoconvection as is readily seen in the figure. Concentration and convection fronts evolve together. This figure can be qualitatively compared with the experimental interferometric concentration curves of Figure 3 from Huth et al.[10] .

Figure 5 shows the logarithmic plot of the simulated anodic convective front, before its collision and merging with the cathodic front, for 0 and 40 percent glycerol. Experimental measurements revealed a transition from a regime when the convective front scales as $t^{4/5}$ at early times to a regime with the front scaling as $t^{1/2}$ for longer times as previously shown. Our simulations reveal the same scaling for both glycerol concentrations and a similar shift in time produced by the viscosity variation.

4 BIPOLAR ELECTROCHEMISTRY

In a typical experiment, when a metallic particle is inmersed in a medium of low conductivity (dilute sulphuric acid solution), the application of an electric field raises potential differences at the borders, because the particle behaves as an equipotential whereas the surrounding medium does not. The applied electric field induces an overpotential on the disc border varying approximately with a cosine law, the maximum value being in the field direction. For a given disc diameter and applied field intensity, two polar regions exist, defined by a critical angle (referred to the field direction) where the electrochemical process takes place. If an electric field is applied to an array of copper discs in an aqueous medium, each disc becomes polarized, and with appropriate electric field strengths, high enough overpotential develop on both sides of the disc and electrochemical reactions take

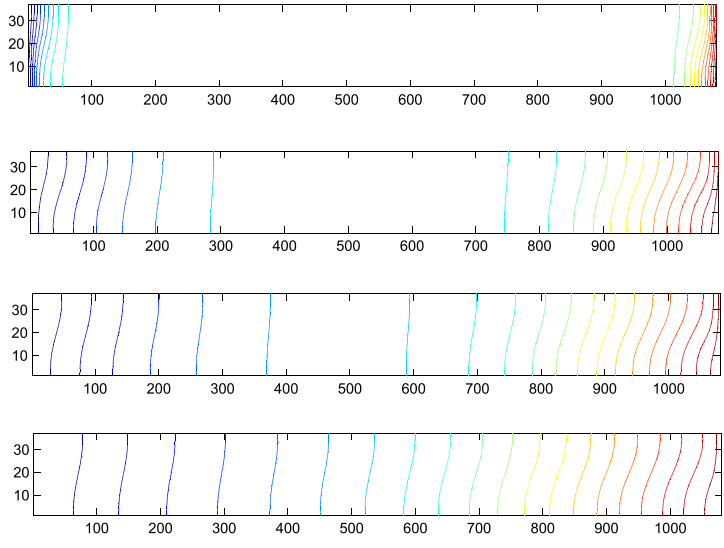

Figure 4: snapshots at different times of cation concentration contours with no added glycerol.

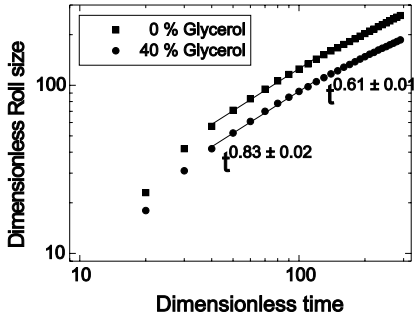

Figure 5: Logarithmic plot of the simulated anodic convective front, before its collision and merging with the cathodic front, for 0 and 40 percent glycerol.

place. On each disc, on the side facing the cell anode, cathodic reactions take place, where as on the opposite side anodic reactions occur. In an array of two discs , in the region between discs along the electric field, one side acts as the cathode and the otheras the anode. In this region, initially copper dissolution takes place on the anodic side whereas hydrogen reduction is produced on the opposite side. After an initial period of time, the copper ion front reaches the opposite copper disc and electrodeposition starts. This time interval is called incubation time. The copper deposit grows preferentially in places where the negative overpotential is largest. When the deposit reaches the opposite copper disc, electrical contact is made, and the potential difference between copper discs and the electrochemical process vanish. This time interval is called contact time. Bradley et al.[4] presented an experimental and theoretical study of SCBE under constant voltage in which the ion transport and its effects on the morphology of the deposit was analyzed. It was shown that the electric field is almost one order of magnitude larger in the region between discs as compared with the mean field value. Moreover, it was shown that the incubation time scales linearly with the inverse of the electric field, and when branching develops, convection plays a relevant role, the contact growing linearly in time with a change of the time/length slope at half the interdisc gap.

The study of thin-layer electrodeposition under alternating voltage conditions and its effects upon morphology has received little attention. In Zeiri et al.,[5] two-dimensional interfacial electrodeposition of silver under alternating square-wave electric potential conditions was studied at the water/dichloromethane interface. They show that the overall deposit growth rate increases with frequency and that the deposit's morphology strongly depends on the frequency: at less than 10 Hz compact deposits are formed while at 1-10 kHz highly ramified structures develop. A pulsating behavior of the deposit size was observed, with alternating contractions and growth phases, attributed to surface tension due to voltage variations which in turn induced hydrodynamical stirring affecting mass-transport of the reacting silver ion to the electrode, and consequently, the rate of growth and morphology of the deposit. D'Angelo et al.[6] conducted a study of SCBE in thin-layer cells under alternating square-wave electric potential conditions. Some of the results corroborated the findings of the work of Zeiri et al.[5] in spite of the different experimental setup. In particular during electrodeposition of zinc, oscillations in the potential, the morphology and the growth speed were observed. Here we review those results.

Figure 6 shows an image superposition of tracked particles in the interval 10-30 s (left) and 30-50 s (right), corresponding to a top view experiment of SCBE under constant voltage. The presence of convection in this stage is clearly seen. The left figure shows the presence of electroconvection as revealed by the curved trajectories. The right one shows also the influence of gravitoconvection. The trajectories are less curved, being the projection of rotation in the plane normal to the growth plane. This rotation is clearly seen during experiment recording.

The forthcoming experiments show the influence of pulsated electrostatic potential over deposit morphology and incubation and contact times. Figure 7 shows a set of top views

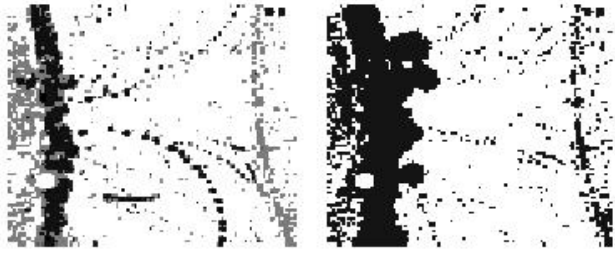

Figure 6: Image superposition of tracked particles in the interval 10-30 s (left) and 30-50 s (right).

of the deposit for DC and frequencies from 0.5 to 400 Hz. The DC deposit in Figure 7 (a) is compared to those of pulsed deposit growth. It is clear that the deposit morphology is substantially affected by the frequency at which the voltage is driven. Figure 7 (b) (0.5 Hz) shows that initially several branches, spanning the whole active side of the cathode, grow uniformily. At a time of 104 s, and approximately half the interdisc gap only one branch remains, winning the race. During the experiment recording, a remarkable effect is observed: a periodic expansion-contraction cycle, in which the deposit advances and recedes in phase with the driving voltage (later addressed). The width of the principal branch is approximately one half of the interdisc gap. A similar evolutionary behavior was observed for 0.75 Hz, although the branching seems less ramified (Figure 7 (c)). The oscillations were also clearly seen during the experiment recording. Figure 7 (d) (3.25 Hz) shows a deposit with only one principal branch. Here, the oscillations observed during growth were much weaker. In Figure 7 (e) and (f) (10 and 400 Hz, respectively) the principal branch is clearly thinner as frequency increases. In Figure 7 (f), the deposit is very compact with no significant secondary branching. Since no oscillations were observed for this frequency, one might be tempted to compare Figure 7 (f) with Figure 7 (a) on the ground that the effect of high frequency will be similar to DC, but of course this is not the case, as it can be seen by inspection of both figures which are quite different. In fact, DC growth is much more similar to growths obtained at low frequencies (compare, for instance, Figures 7 (a) and (d)). The reason is that at low frequencies, the on half-cycle is sufficiently long as to resemble DC, yielding similar growth. We may conclude that at low frequency, the deposits are highly ramified, while at higher frequencies are less branched, even less ramified than under DC conditions.

5 THEORETICAL AND NUMERICAL MODELING IN BIPOLAR ELECTROCHEMISTRY

In the following we analyze SCBE behavior under constant voltage control by distinguishing two well - defined stages: an incubation period with no deposit growth and a growth period where the deposit grows and eventually contact is established. Electroneutrality is assumed and we focus on the study of the electric field distortion due to the presence of copper particles. Clearly, this is a first step towards a more realistic description of SCBE in which the electroneutrality assumption is removed and full ion transport is taken into account. This scenario can be modeled theoretically with the macroscopic model presented in a previous section with appropiate boundary conditions and an appropriate aggregation model for the growth process. We consider a top view model of the SCBE experiment, that is, a model describing SCBE in the quasi-plane of the growth (the plane containing electrodes and discs). Inside the metal discs the electric potential is constant, whereas outside it is variable. Thus, a position dependent potential difference will arise at the disc/solution interface, being zero (by symmetry considerations) at the disc diameter normal to the field direction and maximum at the disc diameter parallel to the field direction. In the event that the interfaces were to be polarized, the maximum overall

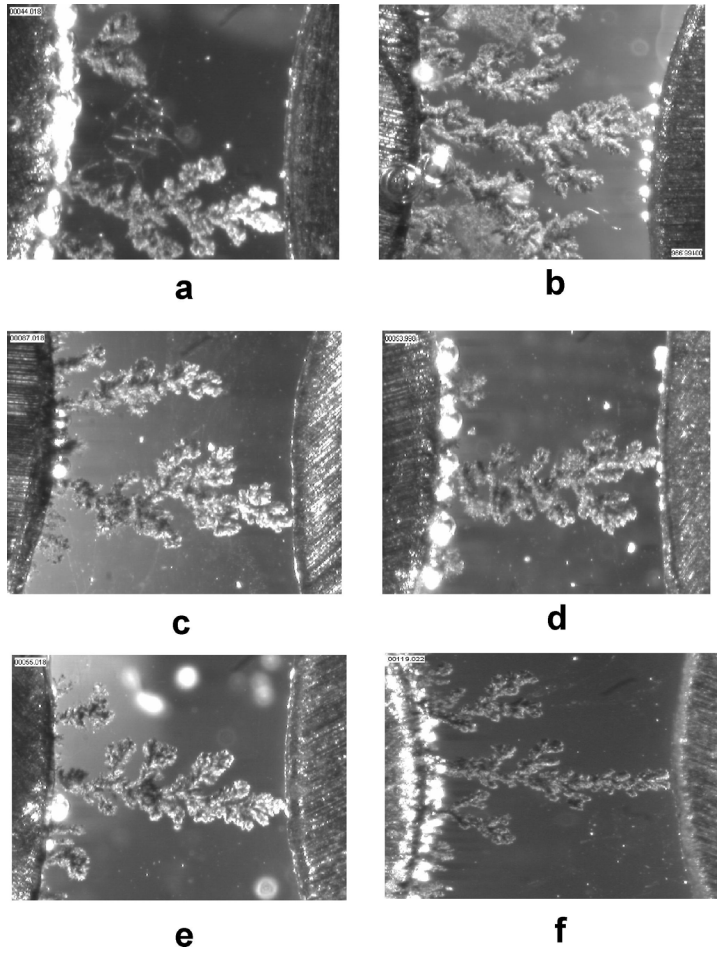

Figure 7: Top view of the deposit obtained for different frequencies: (a) DC; (b) 0.5 Hz; (c) 0.75 Hz; (d) 3.25 Hz; (e) 10 Hz; (f) 400 Hz.

overpotential would be the mean electric field times the disc diameter.

Based on previous considerations we can now calculate the initial potential profile as follows. In the initial stage, electroneutrality holds, and diffusive and convective effects are absent; then, we can write for a top view model mapped in a two-dimensional region in the $x - y$ plane:

$$\nabla \bullet \mathbf{J} = 0 \tag{6}$$

where $\mathbf{J} = \kappa(x, y)\mathbf{E}$ is the current density, $\mathbf{E}$ is the electric field and $\kappa(x, y)$ equals copper conductivity inside the discs ($\kappa = 6 \times 10^7$ S cm^{-1}) and solution conductivity ($\kappa = 5 \times 10^{-3}$ S cm^{-1}) elsewhere, assuming uniform concentration. This leads to the following Laplace-type equation for the electrostatic potential

$$\frac{\partial}{\partial x}(\kappa(x, y)\frac{\partial \phi}{\partial x}) + \frac{\partial}{\partial y}(\kappa(x, y)\frac{\partial \phi}{\partial y}) = 0 \tag{7}$$

The boundary conditions are fixed potential at the electrodes ($\phi = 0$ at $y = 0$ and $\phi = V$ at $y = 1$) and insulating boundaries at the sides of the cell ($\mathbf{J} = 0$ at $x = 0$ and $x = 1$).

Equation (7) is solved in a uniform rectangular lattice of size h (space step), using finite differences and deterministic relaxation techniques. Copper discs are defined by the set of points $P(x_i, y_i)$ satisfying $(x_i - X_{0,k})^2 + (y_i - Y_{0,k})^2 \leq r_{0,k}$, where $r_{0,k}$ ($k = 1, 2$ is the disc index) are the corresponding disc radius and $X_{0,k}, Y_{0,k}$ are the discs centers.

In the numerical simulations shown next we use the physical constants and cell geometry corresponding to the experiments presented in the previous section, assuming uniform concentration. A top view model of the cell geometry, electrodes and copper discs is mapped into a rectangular lattice of 260x360 nodes. The space step is 0.01 cm. The line joining the discs centers is aligned with the electric field. The disc centers are located at points with coordinates (120, 140) and (120, 190), respectively, The gap between copper discs is 10 nodes.

Figure 8 and 9 show the simulated electric field and equipotential lines for different spike lengths. The former simulates a spike of length equal to 30 percent of the interdisc gap, the latter, 70 percent of the gap length. The arrows indicate the direction and intensity of the electric field. The concentration of field lines at the spike tip are clearly visible.

Numerical simulations of pulsated SCBE (not shown) uses a similar technique as that for SCBE under constant voltage control, except the boundary conditions, which are adjusted to the corresponding pulsated voltage. Simulations reveal that in the one-half cycle the electric field is approximately one order of magnitude larger in the intergap region as compared with the mean field value.

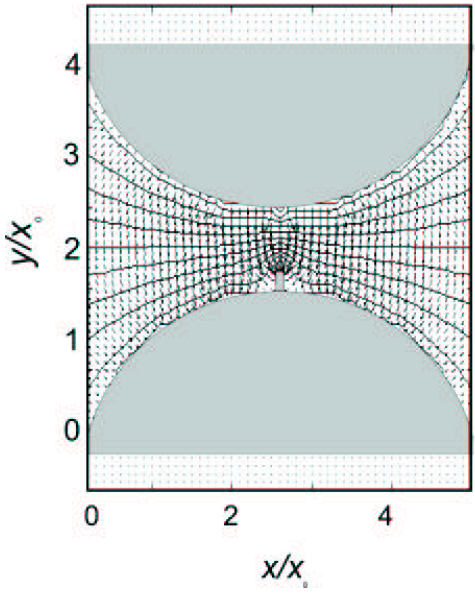

Figure 8: Simulation of the electric field and equipotential lines for a spike length equal to 1/3 of the interdisc gap.

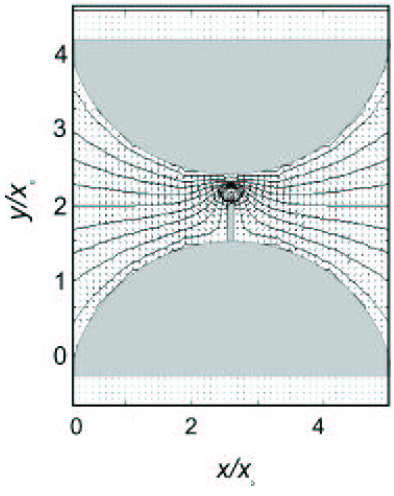

Figure 9: Simulation of the electric field and equipotential lines for a spike length equal to 3/4 of the interdisc gap.

6 DISCUSSION

In a typical monopolar ECD experiment under constant electric field, when the circuit is closed current starts flowing through the electrolyte and, in an initial period, ion concentration boundary layers develop near both electrodes. At the anode, the concentration is increased above its initial level due to the transport of anions towards, and the dissolution of metal ions from the anode. At the cathode, the ion concentration is decreased as metal ions are reduced and deposited out and anions drift away. These concentration variations lead to density variations, and so to the development of gravity-driven convection rolls or vortex tubes at the electrodes. Simultaneously, in a very narrow region near the cathode a local charge develops, giving rise to Coulombic forces initially pointing towards the cathode. After the initial period, an instability develops, triggering the growth of a deposit evolving as a three-dimensional array of thin porous metallic filaments. Coulombic forces concentrate at the tips; each filament allows fluid to penetrate its tip and to be ejected from the sides, forming a toroidal vortex ring driven by the electric force.

Computational modeling, based on a macroscopic model describing ion transport, electrostatic potential and fluid flow, allow the prediction of fronts interaction, vortex generation and merging and the computation of concentration, electrostatic potential and velocities variations. In particular, convection fronts initially grow in size as $t^{4/5}$, where t is the time, while at later times the growth crossed over to a $t^{1/2}$ growth law, the same scaling as observed in the experiments. In the theoretical model the equations are written

in terms of 13 dimensionless numbers showing the significance of the gravity Grashof number in gravitoconvection prevailing regimes. When ramified deposits form, they interact with the gravity current: the vortex tube bends and surrounds filaments, forming a sort of three-dimensional envelope tube squeezed by the filament tip and slaved to the deposit front. The interaction among vortex rings due to coulombic forces and vortex tubes due to buoyancy driven forces in the presence of ramified deposits and their collision with the anode vortex tube is a complex, three-dimensional problem presently under study[15] .

In a typical monopolar ECD experiment when viscosity is increased through glycerol additions, measurements reveal that convection decreases, concentration profiles are less pronounced, while electric resistance and voltage increase. Convective fronts slow down with viscosity, but their time scaling follows the same law as for solutions without glycerol, only differing by a constant. Velocity measurements reveal that increasing viscosity the intensity of gravitoconvective motion decreases, while electroconvection becomes relatively stronger. In the theoretical model the influence of viscosity is manifested through the variation of the Migration, Peclet, Poisson, Reynolds and electrical Grashof numbers. The theoretical model predicts the same scaling as in the experiments, when viscosity is increased.

In a typical bipolar electrodeposition experiment in thin-layer cells (SCBE) under constant electric fields, when the circuit is closed, potential differences develop between external electrodes, and in the interdisc region in both metal mid solution interfaces. On the anode nearest disc, copper dissolution takes place, thus working locally as anode. On the opposite disc border hydrogen gas evolves, being the cathode of the interdisc gap. A copper ion front thus generated moves towards it, and upon arriving copper deposition starts. In the incubation period, ion concentration boundary layers develop near both electrodes. At the anode, the density is increased above its initial level due to the transport of anions towards it and to the dissolution of copper ions from the disc. At the cathode, the density is decreased as hydrogen ions are reduced and anions drift away. These density variations lead to the development of gravity-driven convection rolls at the disc borders. Motion is observed experimentally in the interdisc region, even with the dilute solutions employed, where high density variations are not expected. In ECD, ion transport is caused by a complex interplay of migration, diffusion and convection, the latter mainly driven by electric and buoyancy forces. However, it is found here that in the first stages of the process, during incubation time, ion transport is mainly governed by migration. This is based upon the observation of particle trajectories in the first stages of the process that follow the electric field path, rather than closed orbits (an indication of electroconvective vortex motion) and by the linear relationship found between the inverse incubation time and the electric field. When the ionic copper wave reaches the cathodic side, deposition starts with a dendritic morphology, growing towards the anode exhausting the copper ions in its way. It is conjectured that, as in the case of ECD, as the metal ions are reduced, further density variations lead to increased gravity driven convection rolls. Simultaneously, charges surrounding the tips of the deposit branches interact with

the increased electric field and the electrokinetic effect generates vortex pairs that push ions towards the tip and drag fluid along. Electroconvective vortices rotate in the quasi-plane of the discs, in contrast with gravity driven rolls which rotate in a perpendicular plane (vertical plane). When the ramified deposit forms, it interacts with gravity driven rolls and electroconvective rolls, these strongly influencing its growth and shape. As in monopolar ECD, the interaction of vortex rings produce a complex three-dimensional helicoidal motion whose projection is observed in Figure 9.

The two main stages in the SCBE process, incubation and growth, have been analysed. During the first stage, copper ions migrate in the interdisc region towards the cathodic side. In the second stage, the characteristics of the growth process are similar to those observed in ECD. Numerical simulations of the electric field, in particular in the interdisc region, allow the analysis of the incubation time. It is found that the ion transport prevailing mode is migratory. The incubation time, under the conditions studied here, results inversely proportional to the electric field. During the growth period, experiments reveal a transition in growth rate and morphology appearing at mid distance between copper discs. It is conjectured that this transition is related to a change from a migratory controlled to a convective controlled ion transport mode. Gravitoconvective fluid motion is observed to start during the first stage and to increase in the second one. In this last stage, experiments reveal electroconvective motion near the growing tip. It is conjectured that during this period convection has a relevant role as an ion transport mode and on the deposit growth and form.

In a typical bipolar electrodeposition experiment in thin-layer cells (SCBE) under pulsated electric fields, the previous phenomenological description applies during the on half-cycle. In the off half-cycle, concentration gradients relax diffusively as potential gradients turn off, and, as observed in the experiments, inertia effects are negligible, at least at low frequencies. The AC frequency influences SCBE experiments: the deposit morphology is found to depend on frequency. The incubation time doubles that found in DC experiments, with little dependence on frequency. At low frequencies the ion transport and the deposit growth were observed to pulsate in phase with the electric potential. At the scale of the observation (10x), no signs of inertial effects were discerned. This indicates that electroconvection dominates over gravitoconvection during the deposit growth stage. The general behavior observed can be explained as a competition between the processes occurring during the on and off half cycles. In the former, electrochemical reactions take place and all transport modes are present. In the latter, no reactions occur and concentration gradients rela through diffusion, which is here the predominant transport mode. It is found that the deposit morphology becomes less ramified as frequency increases, while the deposit growth speed is not significantly affected.

The model simulations for pulsated SCBE show that in the on half- cycle the electric field is almost an order of magnitude larger in the region between discs as compared with the mean field value, as in the constant field case.

ACKNOWLEDMENTS: G. M. is thankful to the Fulbright Commission for a scholar-

ship. G. M. and F. V. M. are investigators of the CONICET, Argentina. G. G. and S. D. are supported by CONICET and University of Buenos Aires, respectively. This work was partially supported by UBA Grant No. TX09/99, FOMEC Grant No. 376/98 from the Department of Computer Sciences, FCEyN, UBA and CONICET grant No. PIP379/98.

REFERENCES

[1] A. Sawada, Y. Dougherty, and J. P. Gollub. *Phys. Rev. Lett.*, **56**, 1260 (1986).
[2] G. Gonzalez, G. Marshall, F. V. Molina, and S. Dengra. *Phys. Rev. E*, page 051607 (2002).
[3] J. C. Bradley, H. M. Chen, J. Crawford, J. Eckert, K. Ernazarova, T. Kurzeja, M. Lin, M. McGee, W. Nadler, and S. M. Stephens. *Nature*, **389**, 268 (1997).
[4] J. C. Bradley, S. Dengra, G. A. Gonzalez, G. Marshall, and F. V. Molina. *J. Electroanal. Chem.*, **478**, 128 (1999).
[5] L. Zeiri, S. Efrima, and M. Deutsch. *Langmuir*, **13**, 4722 (1997).
[6] V. D'Angelo, G. Marshall, J-C. Bradley, G. Gonzalez, S. Babu, F. V. Molina, and C. Iemmi. *Spatially coupled bipolar electrodeposition in thin-layer cells under periodic voltage control, presented at Symposium J1- Morphological Evolution in Electrodeposition, 199th Meeting of The Electrochemical Society (ECS), March 25- 29, 2001 Washington, DC, USA.*
[7] V. Fleury, G. Marshall, and M. Rosso. *Role de la viscosite dans la croissance electrochimique en cellule mince, LPMC, Ecole polytechnique, Palaiseau, France.*
[8] G. Gonzalez, G. Marshall, F. V. Molina, S. Dengra, and M. Rosso. *J. Electrochem. Soc.*, **148**, C479 (2001).
[9] G. Gonzalez, G. Marshall, F. V. Molina, S. Dengra, and A. Sanchez. *The role of viscosity on ion transport in thin-layer electrodeposition, Symposium J1- Morphological Evolution in Electrodeposition, 199th Meeting of The Electrochemical Society (ECS), March 25-29, 2001 Washington, DC, USA.*
[10] J. Huth, H. Swinney, W. McCormick, A. Kuhn, and F. Argoul. *Phys. Rev. E*, **51**, 3444 (1995).
[11] A. J. Bard and L. R. Faulkner. *Electrochemical Methods, Fundamentals and Applications.* (1980).
[12] G. Marshall, P. Mocskos, H. L. Swinney, and J. M. Huth. *Phys. Rev E*, **59**, 2157 (1999).
[13] G. Marshall and P. Mocskos. *Phys. Rev E*, **55**, 549 (1997).
[14] G. Marshall, S. Dengra, E. Arias, F. V. Molina, M. Vallieres, and G. Gonzalez. *Ion transport modeling in realistic thin-layer ECD for gravitoconvection prevailing regimes, Symposium J1- Electrochemical Processing in ULSI fabrication and electyrodeposition on and on semiconductors IV, 199th Meeting of The Electrochemical Society (ECS), March 25-29, 2001 Washington, DC, USA.*
[15] G. Marshall, E. Mocskos, F. Molina, F. Daffara, and S. Dengra. *Beyond Dendrites in ECD, (submitted)*, (2002).

[16] D. Grier, E. Ben-Jacob, R. Clarke, and L. M. Sander. *Phys. Rev. Lett.*, **56**, 1264 (1986).
[17] T. Vicsek. *Fractal Growth Phenomena.* (1992).
[18] R. M. Brady and Ball. *Nature*, **309**, 225 (1984).
[19] D. Barkey. *J. Electrochem. Soc.*, **138**, 2912 (1991).
[20] F. R. McLarnon, R. H. Muller, and C. W. Tobias. *J. Electrochem. Soc.*, **136**, 3630 (1989).
[21] R. H. Cork, D. C. Pritchard, and W. Y. Tam. *Phys. Rev. A*, **44**, 6940 (1991).
[22] P. Carro, S. L. Marciano, A. Hernandez Creus, S. Gonzalez, R. C. Salvarezza, and A. J. Arvi. *Phys. Rev. E*, **48**, 2374 (1993).
[23] P. Trigueros, J. Claret, F. Mas, and F. Sagues. *J. Electroanal. Chem.*, **312**, 219 (1991).
[24] V. Fleury, M. Rosso, J-N. Chazalviel, and B. Sapoval. *Phys. Rev. A*, **44**, 6693 (1991).
[25] V. Fleury, J-N. Chazalviel, and M. Rosso. *Phys. Rev. Lett.*, **68**, 2492 (1992).
[26] V. Fleury, J-N. Chazalviel, and M. Rosso. *Phys. Rev. E*, **48**, 1279 (1993).
[27] C. Livermore and Po zen Wong. *Phys. Rev. Lett.*, **72**, 3847 (1994).
[28] V. Fleury, J. Kaufman, and B. Hibbert. *Phys. Rev. E*, **48**, 3831 (1993).
[29] V. Fleury, J. Kaufman, and B. Hibbert. *Nature*, **367**, 435 (1994).
[30] M. Rosso, J-N. Chazalviel, V. Fleury, and E. Chassaing. *J. Electrochem. Soc.*, **141**, 1206 (1994).
[31] D. P. Barkey, D. Watt, Z. Liu, and S. Raber. *J. Electrochem. Soc.*, **141**, 1206 (1994).
[32] V. Fleury, M. Rosso, and J-N. Chazalviel. *Mater. Res. Soc. Proc.*, **367**, 183 (1995).
[33] C. Leger, J. Elezgaray, and F. Argoul. *Phys. Rev. Lett.*, **78**, 5010 (1997).
[34] K. A. Linehan and J. R. de Bruyn. *Can. J. Phys.*, **73**, 177 (1995).
[35] J-N. Chazalviel, M. Rosso, E. Chassaing, and V. Fleury. *J. Electroanal. Chem.*, **407**, 61 (1996).
[36] F. Argoul, E. Freysz, A. Kuhn, C. Leger, and L. Potin. *Phys. Rev. E*, **53**, 1777 (1996).
[37] S. Dengra, G. Marshall, and F. Molina. *J. Phys. Soc. Japan*, **69**, 963 (2000).
[38] N. Hecker, D. J. Grier, and L. M. sander. *Fractal Aspects of materials, R. B. Laibowitz, B. B. Mandelbrot, and D. E. Passoja, Editors, Materials Research Society, University Park, PA*, (1985).
[39] P. Garik, D. Barkey, E. Ben-Jacob, E. Bochner, N. Broxholm, B. Miller, B. Orr, and R. Zamir. *Phys. Rev. Lett.*, **62**, 2703 (1989).
[40] J. R. Melrose, D. B. Hibbert, and R. C. Ball. *Phys. Rev. Lett.*, **65**, 3009 (1990).
[41] M. Rosso V. Fleury and J. N. Chazalviel. *Phys. Rev. A*, **43**, 6908 (1991).
[42] P. Trigueros, J. Claret, F. Mas, and F. Sagues. *J. Electroanal. Chem.*, **312**, 219 (1991).
[43] A. Kuhn and F. Argoul. *Fractals*, **1**, 451 (1993).
[44] A. Kuhn and F. Argoul. *J. Electroanal. Chem.*, **371**, 93 (1994).
[45] A. Kuhn and F. Argoul. *Phys. Rev. E*, **49**, 4298 (1994).

[46] D. Otero, G. Marshall, and S. Tagtachian. *Fractals*, **4**, 7 (1996).
[47] J. N. Chazalviel. *Phys. Rev. A*, **42**, 7355 (1990).
[48] G. Marshall, S. Tagtachian, and L. Lam. *Chaos, Solitons and Fractals*, **6**, 325 (1995).
[49] G. Marshall, E. Perone, P. Tarela, and P. Mocskos. *Chaos, Solitons and Fractals*, **6**, 315 (1995).
[50] G. Marshall, P. Mocskos, and M. Olivella. *Mater. Res. Soc. Proc.*, **407**, 355 (1996).
[51] G. Marshall, P. Mocskos, F. Molina, and S. Dengra. *Mater. Res. Soc. Proc.*, **451**, 147 (1997).
[52] J. C. Bradley, J. Crawford, K. Ernazarova, M. McGee, and S. M. Stephens. *Adv. Mater.*, **9**, 1168 (1997).
[53] J. C. Bradley, J. Crawford, M. McGee, and S. M. Stephens. *J. Electrochem. Soc.*, **145**, L45 (1998).
[54] J. S. Newman. *Electrochemical Systems.* (1973).
[55] V. G. Levich. *Physicochemical Hydrodynamics.* (1962).